9

The Use of Power Spectrum Density for Surface Characterization of Thin Films

Fredrick Madaraka Mwema[1,*], Esther Titilayo Akinlabi[1] and Oluseyi Philip Oladijo[1,2]

[1]Department of Mechanical Engineering Science, University of Johannesburg, Auckland Park, Kingsway Campus, Johannesburg, South Africa
[2]Department of Chemical, Materials and Metallurgical Engineering, Botswana International University of Science and Technology, Palapye, Botswana

Abstract

A step-by-step framework for undertaking PSD characterization of the surface topography of radio frequency (rf) magnetron sputtered thin Al films is presented in this chapter. The work aims to illustrate the significance of PSD method in analyzing the surface properties of thin films based on AFM imaging. It also aims at illustrating a repeatable procedure for undertaking PSD analysis on thin films. Brief theoretical background of power spectral density, with highlights on the fundamental theory, is herein presented. A two-dimensional power spectral computation of thin Al films sputtered on a titanium substrate at 150 W and 200 W rf powers for 2 hr is undertaken. Prior to the computation, a detailed image analysis theory and procedure of the AFM micrographs are presented. The calculation of power densities of the AFM images is conducted using the fast Fourier (FFT) algorithm of discrete Fourier transformation (DFT) in MATLAB script. The power spectral results are then fitted into k-correlation and inverse power models to interpret the spectral profiles. From the modelling, the equivalent root means square, correlation length and Hurst components have been determined. These values were distinctly discussed in relation to the sputtering power and morphological observations of the 3D AFM microscopy. The PSD results correlate well with the morphological observations of the atomic force microscopy.

Keywords: Atomic force microscopy, fourier transforms, power spectral density, surface roughness, thin films

**Corresponding author:* fredrick.mwema@dkut.ac.ke

Xiao-Yu Yang (ed.) Photoenergy and Thin Film Materials, (379–412) © 2019 Scrivener Publishing LLC

9.1 Introduction

The connection between the surface topography and functionality of thin films is critical for components used in electrical, optical, mechanical and thermal applications [1, 2]. Roughness is a significant property of thin films as it affects their surface properties such as adhesion, friction and hydrophobicity [3] besides the common mechanical properties; fatigue and fracture toughness [2]. As such, characterization of thin films surface is very important at the quality control stage of any production process for those components to achieve their desired functionality [4, 5]. Some of the standards for surface measurement and control of roughness include ISO 25178, ASTM D7127–13, JIS B 0601–2001/JIS and B 0671–2002 and these standards are based on different measurement methods among them includes x-ray reflectometry (XRR), atomic force microscopy (AFM), profilometry and laser interferometry [6]. Among these measurement techniques, AFM is the most preferred technique because of its low vertical noise and high lateral resolution. AFM uses a sharp-tipped cantilever to scan surfaces and a laser beam monitored by a position sensitive photodiode to detect the deflections of the tip resulting from the topographical changes. It produces surface micrographs at atomic resolution (with less than nanoscale), with the minimum preparation of the surface of the specimen. It can provide images for surfaces in both air and liquid media without any special preparation as it is the case with other techniques. As such, besides metallic and coating surfaces, AFM is widely used in studying the topography of gas and filtration membranes [7]. From these images, the morphology, particle size distribution and porosity of the surfaces can be described [8] and therefore AFM is an important tool for surface analysis.

AFM images are usually used to statistically characterize the surface topography in terms of root mean square roughness (σ), which represents the height function of the surface structures. To illustrate the concept of root mean square roughness, let us consider Figure 9.1 which shows height maps of two different surfaces. The arrows indicate the mean plane of the height of the surface structures. Through visual inspection, structures of the surface in Figure 9.1(b) have a larger deviation from the mean plane. Hence, the root means square roughness in Figure 9.1(b) is higher than in Figure 9.1(a). Let us consider, Figure 9.2(a), (b) in which the root mean square roughness analysis of structures shows that both surfaces have the same root mean square roughness values. However, this is deceiving because it can be observed that the surface in Figure 9.2(a) appears rougher than the surface represented in Figure 9.2(b). Although the structures in

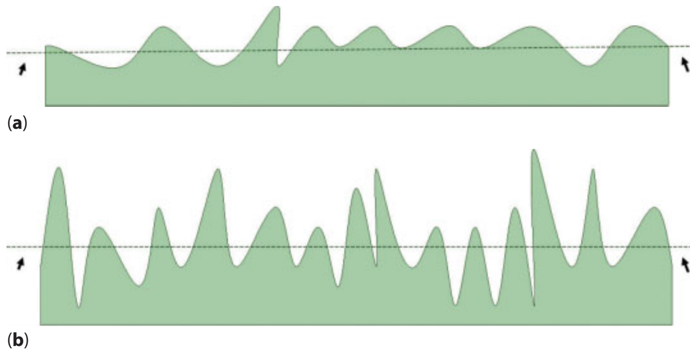

Figure 9.1 Typical surfaces of materials. The arrows indicate the mean plane of the height of the surface structures.

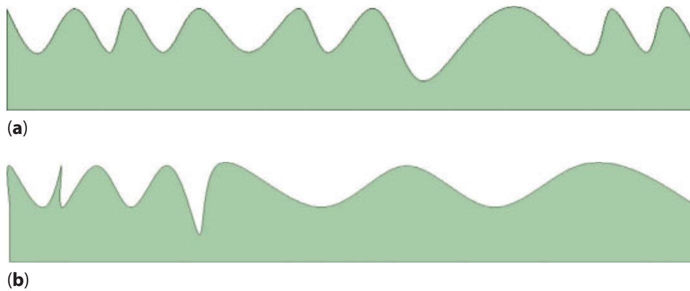

Figure 9.2 Surfaces with the same value of root mean square roughness but with different lateral topography.

both surfaces have the same height deviation from the mean plane, the horizontal arrangement of the surface structures is different. This lateral deviation is the reason for the difference in the appearance of the surfaces and it is the major drawback of the root mean square roughness value. Root mean square roughness does not provide lateral information of surface features (lateral spacing and distribution) and makes no distinction between peaks and valleys, thus, two surfaces can have the same value of σ but have very different surface topographies as illustrated in Figure 9.2(a), (b). Additionally, the statistical values of the root mean square roughness are greatly influenced by sampling interval, scanning scales and other specific aspects of the AFM measurement. Such factors increase the chances of error in the roughness values [9].

A better description of surface geometries is provided by fractal methods such as power spectral density (PSD) functions [9] and have been used by different researchers to describe the surface topography of surfaces of

materials [10–12]. These methods provide information about the lateral distribution of the surface structures, thereby overcoming the limitations associated with root mean square method. PSD computes quantitative topographical parameters such as fractal dimension, Hurst exponent, equivalent roughness values and spectral length. In contrast to the root mean square methods, these PSD quantities are independent of scan rate, scanning cycles, resolution and other AFM measurement parameters [9]. PSD uses Fourier transform theory to change the AFM images into the frequency domain in which the distribution of the surface height with wavenumbers is described. In addition, it identifies the wavelengths of surface features that contribute to surface topography [13]. Through PSD analysis, the information on correlation length can be obtained to indicate the lateral distribution of the valleys and peaks of the surfaces. Mathematically, PSD is the Fourier transform of the autocorrelation function of power signal within a range of wavevectors and it allows for identification of the spatial frequencies in the signal [13].

The purpose of this chapter is to demonstrate a detailed step-by-step application of power spectral density on surface analysis of thin films. The procedure is illustrated using AFM micrographs of thin aluminium films prepared by rf magnetron sputtering on titanium substrates at 150 W and 200 W rf powers. The chapter details the pre-processing procedure for AFM images using Bruker Nanoscope V530r3sr3 and Gwyddion software prior to spectral analysis. The power spectrum computation of the pre-processed images is undertaken using two dimensional fast Fourier transform algorithm in MATLAB code.

9.1.1 Uses of Power Spectral Density

Power spectral density (PSD) expresses the amplitude of roughness of surfaces as a function of the inverse of the wavelength of surface structures. It shows the periodic surface features that might otherwise appear random and then provides their graphical distribution. It enables the characterization of periodicity and orientation of other surface features besides the roughness by revealing the wavelengths contained in the surface spectrum [13]. In thin films, PSD is helpful in describing the lateral roughness, fractal dimensions and homogeneity of the surface structures. On machined surfaces, it determines the speed, feed, causes of noise and the inherent properties of the material surface such as grains. When PSD is used in analyzing high magnification images of surfaces (such as TEM and FESEM micrographs), it determines the periodicity of the atoms. PSD functions generally decompose the surface features of the original image into wavelengths

in imaginary space [12]. For an ideal 2-dimensional image of a surface with two waveforms in X – and Y- directions in the Cartesian space, a PSD function would consist of two dominant spikes each corresponding to the X- and Y- dominant waveforms. There would also be a shorter number of wavelengths inherent in the image resulting from the very fine surface features or from side bands of the two main wavelengths. Usually, surfaces with such perfect sinusoidal features would result in relatively very few spatial frequencies describing the surface, however, for a surface with square or angular waveforms would contain more components of the wave vectors [14]. In machined surfaces, wavelengths containing higher power densities indicate machining irregularities such as microgrooves, cracks and protuberances [14]. Plastic deformation, varying cutting temperature and micro-cracks lower the quality of surface machining of components and results in random (rough) surfaces and the PSD function for such surfaces would exhibit many wavelengths [14].

9.1.2 Theory of Power Spectral Density

Suppose the topography of a surface within a Cartesian space (x, y) is described by a continuous function $z(x, y)$. Let the lengths of the scan in x and y directions be described by L_x and L_y respectively. If we define, f_x and f_y as the wave vectors (spatial frequencies) in x and y directions respectively and note that the function $z(x, y)$ does not include overhangs, then the Fourier transform of this function (Z_{fxfy}) is non-zero only at the discrete lattice points. The forward Fourier transformation of the function is obtained using Equation 9.1 [13].

$$Z_{fxfy} = \int_{L_xL_y} z(x, y)\, e^{-i(f_x x + f_y y)}\, dxdy \tag{9.1}$$

The integration is computed over the full area L_xL_y of the entire periodic surface at steps of $\frac{2\pi}{L_x}$ and $\frac{2\pi}{L_y}$ runs from negative and positive infinity. From this expression, the units of the PSD (Z_{fxfy}) is m^3. This is the case for a continuous function $z(x, y)$ of the surface topography. However, the function exists as discrete points on rectangular grids (Figure 9.3). The discrete points occupy rectangular grids of pixel sizes l_x and l_y in x and y directions respectively in the Figure 9.3. If the number of grids in x and y directions are N_x and N_y respectively, then $l_x = \frac{N_x}{L_x}$ and $l_y = \frac{N_y}{L_y}$ and the Fourier transformation of the function can be obtained by Equation 9.2. This is known as discrete Fourier

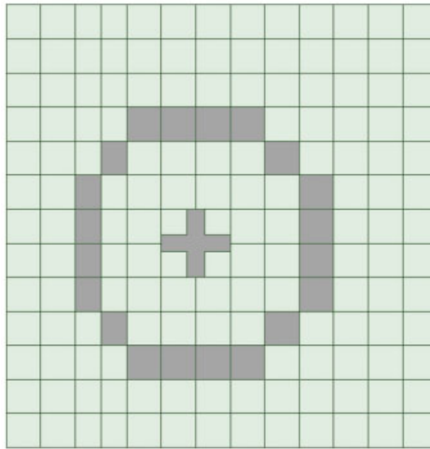

Figure 9.3 Discrete points on rectangular grids as is the case for a real image.

transform (DFT). Usually, during implementation of DFT algorithm, $l_x = l_y = 1$ and $L = N$ in both directions.

$$Z_{fxfy} = l_x l_y \sum_{x,y} z\left(x,y\right) e^{-i\left(f_x x + f_y y\right)} \tag{9.2}$$

Equations 9.1 and 9.2 are the basis of PSD derivation and all the PSD models are based on these equations. Generally, $2D\ PSD = \frac{1}{L_x L_y}\left|Z_{fxfy}\right|^2$ and directly using equation 9.2, 2D PSD can be written as shown in Equation 9.3. The units of the 2D PSD from this expression is m^4.

$$2D\ PSD = \frac{1}{L_x L_y}\left|l_x l_y \sum_{x,y} z\left(x,y\right) e^{-i\left(f_x x + f_y y\right)}\right|^2 \tag{9.3}$$

The variation in PSD computation methods presented in the literature is brought about by the different normalization procedures.

For instance, a finite N number of values in discrete space are assumed to be equidistantly positioned in x, y directions at distances $x, y = \frac{L}{N}$. The 2D PSD can be written as in Equation 9.4 [11].

$$2D\,PSD = L^2\left[\frac{1}{N^2}\sum_{n=0}^{N}\sum_{m=0}^{N} z\left(x_m, y_n\right) exp\left(2\pi j.x_m f_x\right) exp\left(2\pi j.y_n.f_y\right)\right] \tag{9.4}$$

Where $x_m = m.\frac{L}{N}$, $y_n = n.\frac{L}{N}$ and f_x, f_y take a discrete range value as $f_x, f_y = \frac{1}{L}, \frac{2}{L}, \ldots\ldots\ldots.\frac{N}{2L}$

Equation 9.5 represents another method for computation of PSD for an image of m (along x-axis) by n (along with y-axis).

$$PSD_{(f)} = \frac{2d}{N}\left[\sum_{n=1}^{N} e^{\frac{2\pi i}{N}(n-1)(m-1)} Z(n)\right]^2 \text{ for } \quad \mathrm{f} = \frac{\mathrm{m}-1}{\mathrm{Nd}}; \quad \text{2D PSD} = \frac{\text{PSD}}{2}\mathrm{f}\left(\Delta \mathrm{f}\right) \tag{9.5}$$

Where frequencies range from $\frac{1}{L}$ to $\frac{N}{2L}$, N is the scan size in pixels and d is the data points intervals while $Z\left(n\right)$ is the roughness height function of the surface structures.

Another form of PSD in which h_{mn} is the profile function and $L = \frac{L}{N}$ is illustrated in Equation 9.6 [15]. This equation undertakes both fast Fourier transforms of the image signals and computation of the two-dimensional power spectral densities. The computation is based on *m* and *n* array of discrete points in *x* and *y* directions of the global coordinate system. It performs quicker computation and a typical application for discrete Fourier transform (DFT) algorithm.

$$2D\ PSD = \frac{1}{L^2}\left[\sum_{n=1}^{N}\sum_{m=1}^{N} h_{mn}\exp - \left(2\pi i.L\left(\mathrm{m}f_x + \mathrm{n}f_y\right)\right)\left(L\right)^2\right]^2 \tag{9.6}$$

Most thin films are self-affine due to the same statistical characteristics at different magnifications or scales. When PSD computations of such surfaces are computed with the equations described here and plotted against the wave vectors (loglog axis), profiles like those illustrated in Figure 9.4 are obtained. Generally, profiles for randomly rough surfaces in Figure 9.4(a) exhibit a plateau and an inverse slope at low and high spatial frequencies respectively with a knee at the transition zone [16]. The physical meaning of the plateau is that there is no significant variation in the values of the roughness function at low frequency whereas below the transition point (higher frequencies) the roughness varies in a highly correlated manner [11]. At the longest wavelength, f_1, the root mean square amplitude can be determined whereas the average slope is determined by the shortest wavelength (f_2) of the roughness function.

To undertake mathematical descriptions of the roughness characteristics of surfaces from PSD profiles, various theoretical models into which the experimental PSDs are fitted exist. The most commonly used models are k-correlation model (also known as ABC model) and inverse power law (or fractal model). Equation 9.7 represents the k-correlation model power spectral density [9].

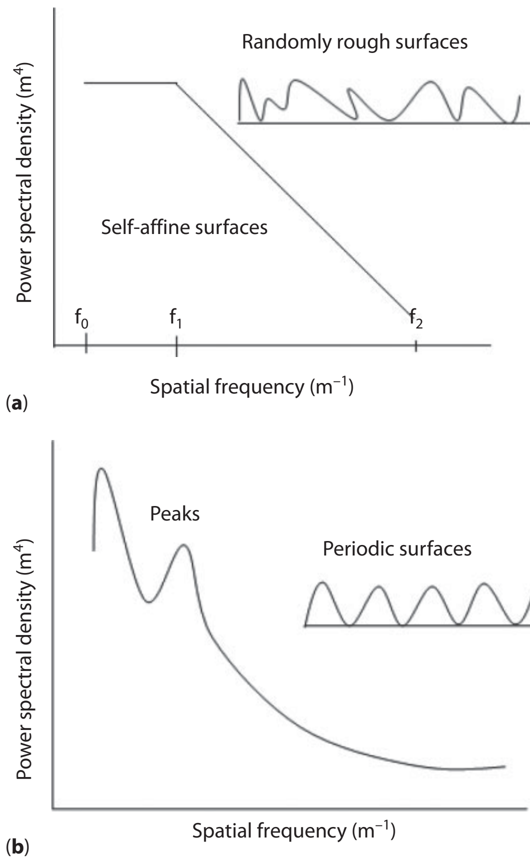

Figure 9.4 A typical PSD versus spatial frequency profiles for (a) randomly rough surfaces and (b) periodic surfaces.

$$PSD = \frac{A}{\left(1 + B^2 f^2\right)^{\frac{(C+1)}{2}}} \tag{9.7}$$

The k-correlation model is most suitable for pure thin films and explains the random distribution of topography characteristics at large length scales. A, B and C are the fitting constants of the k-correlation function and provide physical derivatives of the power spectral density. The function gives a PSD profile with a knee, described by parameter B. The value of B indicates the location of the knee and it is related to in-plane correlation length and grain size. It describes the transition from low to a high spatial frequency region. At higher spatial frequencies, the slope is described by C

and at that region, the surface said to be fractal. Parameter A, also known as shoulder parameter, is the value of the spectrum at low frequency and at that region the power spectrum nearly flat. In the two-dimensional fast Fourier transform (2D-FFT) spectrum, the value A is associated with the peaks or large features of the real AFM micrograph.

The equivalent roughness (**σ**) and correlation length (**τ**) according to the k-correlation model are given as $\sigma_{ABC} = \frac{2\pi A}{B^2(C-1)}$ and $\tau = \frac{(C-1)^2 B^2}{2\pi^2 C}$ respectively. The inverse power law is expressed as shown in equation 9.8 where K is the spectral length and γ is the gradient of the loglog graphs. Self-affine surface with roughness Hurst exponent H are usually described by power or fractal model at high spatial frequencies. The Hurst exponent is related to fractal dimension D as $H = 3 - D$. It describes the process used in forming the measured surface and it usually varies between 0–1. The exponent indicates the spatial distribution of roughness of a surface; usually, if H varies between 0–0.5, it means that the spatial frequency of the surfaces is continuously alternating between high and low values, which indicates uniform roughness distribution. However, when H is greater than 0.5, it indicates spatial frequencies with positive autocorrelation, meaning there are sudden changes in surface features and nonuniform distribution of roughness [9].

$$PSD = \frac{K}{f^{\gamma}} \tag{9.8}$$

9.2 Literature Review

In this section, the progress of surfaces analysis using power spectral density is presented. The general agreement in literature is that fractal methods, which define roughness at different spatial wavelengths, can provide reliable measurements of surface topography regardless of measuring method, scale or scan. In their study, Gong *et al.,* [9] reported that using a combined power spectra of different scan scales from AFM micrographs of TipCheck standards generated enhanced correlation lengths for computation of roughness values. Senthilkumar *et al.,* [12] applied a similar approach of extended PSD analysis on the microroughness characterization of thin films of Gd_2O_3 and obtained reliable roughness values which related very well with the process deposition rate. Karan and Mallik [15] used PSD analysis fitted with a k-correlation model to derive the fractal contributions into the morphological growth of CuPc nanostructured thin films deposited on Si at different substrates. Anandhan, Bandyopadhyay

and Bhowmick [17] used one-dimensional PSD to quantify the surface geometry of thermoplastic elastomers and computed the fractal dimensions (D_s) from the slope (D) determined by linear fitting into the self-similar constant gradient region of the PSD profiles. The fractal dimensions were determined as follows $D_S = D$ and they were shown to vary from 2 to 3. In another study, Buchko *et al.,* [18] used the concept of PSD computed from scanning probe microscopy to study the effect of the process parameters on the surface topography of protein polymer thin films for biomedical applications. Using the PSD profiles, the periodicity and average sizes of surface features such as pores were quantified. The peaks of the PSD profiles at the transition region (low-to-high frequency) were interpreted to correspond to the average sizes of the surface pores of the protein films. The PSD profiles were also shown to explain the transition of the self-affine roughness to nominally smooth [18]. The study also used power law exponent within the self-similar region of the PSD profiles to compute the fractal dimensions of the thin films.

In a rather recent study, power spectral density characterization was undertaken on AFM micrographs of thin aluminium films deposited through rf magnetron sputtering on stainless and mild steel substrates at 150 W and 200 W [19]. In this study, the power spectral density modelling was undertaken through k-correlation (ABC model) and fractal (power law) analyses at low and highfrequency regions respectively of the PSD profiles. The implications of domination of power law to power density were presented in details in this article [19]. The lateral distribution of the surface roughness was discussed quantitatively using Hurst exponent determined from the k-correlation model. In a related study [11], one dimensional PSD spectra computed from AFM micrographs were used to study the microstructural properties of thin titanium oxide films prepared on glass substrates by DC magnetron sputtering at different substrate temperatures. K-correlation modelling was used to derive the physical meaning of the PSD profiles and parameters A, B and C were shown to fully describe the microstructural evolution of titanium oxide films with substrate temperature during sputtering. A study by Datta, Bhattacharya and Bandyopadhyay [20] used power spectral density to analyze surface roughness distribution and growth of surface structures of CdSe thin films prepared by cathodic deposition on a glass substrate at a temperature range of 100–140°C. Higher values of wavelengths of the power spectral density were observed at 100°C and 140°C than the intermediate temperatures. These observations were attributed to agglomeration of crystallites at 100°C and 140 °C, which led to the formation of larger surface structures and non-homogeneous lateral roughness [20]. Microstructural

characterizations of the TiO_2 and $Pb(ZrTi)O_3$ prepared through reactive sputtering were studied by power spectral density modelling using k-correlation model [21]. It was possible, through PSD technique, to demonstrate that the fractal dimensions of thin films' surfaces are influenced by the processing conditions. Aurongzeb [22] explored the evolution of scaling properties of Ti films (prepared through electron beam evaporation) during annealing at various temperatures using PSD. The relationship between surface roughness and an annealing temperature of Ti films was established in this study.

The preceding discussion illustrates the importance of PSD in detailing the microstructures of thin films in terms of distribution, evolution and growth of surface structures in relation to the deposition and treatment parameters. Although lots of researchers have used power spectral density to analyze thin films, step-by-step descriptions of the PSD approach are lacking in literature and as such, most of the presented results cannot be repeated and reproduced easily. The overall aim of this book chapter, therefore is to provide readers with a typical framework of undertaking power spectral density characterization of thin films.

9.3 Methodology

In this section, a case to illustrate a logical framework for PSD analysis of thin films is presented. The flowchart in Figure 9.5 summarizes the analysis steps used in this work and are detailed in the subsequent subsections.

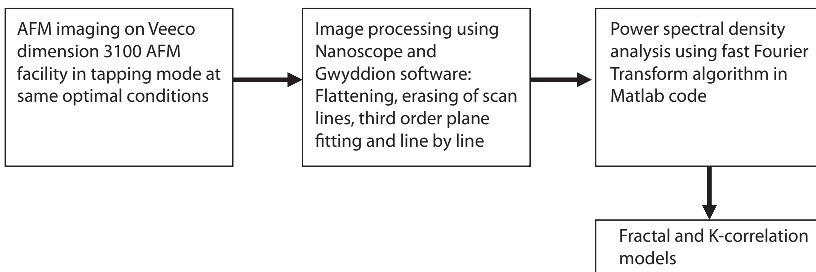

Figure 9.5 Analysis procedure used to process the AFM micrographs for power spectral computation.

Table 9.1 Sputtering parameters and conditions for Thin Aluminum Films on Titanium Substrate.

Parameters	Description
Target	99.9% Al purity, size ∅75 mm, 3 mm thickness
Substrate	Ti6Al4V, CpTi, size 75 × 25×3 mm
Substrate temperature	Room temperature
Time	2 hr
Argon flowrate	12 sccm
Base pressure	1.13×10^{-5} mbar
Rf power	150 W, 200 W

9.3.1 Thin Film Deposition

In this case, aluminum and titanium were used as target and substrates respectively because thin aluminum films are suitable intermetallic coatings for titanium-based alloys [23]. The surfaces of the substrates were ground to 1200 μm SiC grade and then cleaned in acetone to remove any oxides and surface suspensions. The films were prepared through rf magnetron sputtering using HHV TF500 thin film deposition facility under conditions shown in Table 9.1. Prior to sputtering, the substrates were initially cleaned with acetone, isopropanol and dried. The pre-sputtering of the substrate was undertaken for 30 min in which the argon plasma was bombarded on the substrate to clean its surface for effective deposition of the films. The distance between the target and substrate was kept at 130 mm. After sputtering, the samples were left to cool inside the chamber for at least 12 hr. More details of the sputtering process were described in our earlier work [19].

9.3.2 Atomic Force Microscopy

The coated samples were cut into sizes of 10 × 10 mm for atomic force microscope (AFM) imaging. AFM was conducted using Veeco Dimension 3100 AFM facility in tapping mode in air and at room temperature. Tapping mode is preferred for metallic surfaces because it has less effect on the wear of the AFM probe. Standard AFM probe of spring constant of

2.8 N/m with a resonance frequency of 75 kHz was used. The images were taken at a scan size of $3 \times 3\ \mu$m at integral and proportional gains of ranges of 0.4–0.8 and 0.6–1.0 respectively [19]. Due to the large roughness of the surfaces, no image could be observed above this scan size. Scan rate and angle used were 1 Hz and 0 degree respectively. The scan rate should neither be too slow nor too fast; very slow scan speed can result into drifting during longer scanning periods, whereas very fast scan speed can produce an image with elongated (false) surface structures [7]. Through series of trials, 1 Hz was shown to produce an image with less artefacts. The optimal set point (forces) for the images ranged between 0.899 and 1.120 at a drive amplitude of 840 mV. At these conditions, there was less noise on the scope traces for the three images (height, amplitude and phase), indicating optimum conditions for these surfaces [24]. When all the conditions were optimized, five AFM images were taken at different sections of the sample surface at the same gain conditions, scan rate and size for statistical accuracy. The image analyses were performed in Bruker Nanoscope V530r3sr3, Gwyddion and MATLAB (Mathworks®) software.

9.3.3 Image Analysis

9.3.3.1 AFM Image Pre-Processing

Image analysis is used to extract the physical information from an image and in materials science and engineering, it is the extraction of information from a micrograph [25]. Some of the most common information obtainable from a microstructure include morphology, grain size, grain distribution, the area fraction of phases, aspect ratio, ferret number, roughness and sphericity [26]. Similar to SEM and optical micrographs as described by Mwema *et al.,* [26], AFM images have to go through a pre-processing stage to correct for artefacts and map the important features for measurement before the actual image analysis. Some of the AFM sources of artefacts include nonlinearity of the piezo-scanner and hysteresis, physical damage of the surface by the scanner and convolution of the tip and sample shapes in the obtained image [7]. In this work, the Bruker Nanoscope software (Version 530r3sr3) was used to collect the AFM micrographs and calculate the root mean square and average roughness values of the surfaces. Prior to analysis, flattening and third order plane fitting was undertaken on all AFM images. Line by line flattening was performed to remove vertical offsets, noise, tilt and other unwanted features from the AFM image. These artefacts are the result of tilting of the sample, cleaving of the substrate or the AFM voltage offset. The flattening feature uses least square

Table 9.2 Plane fitting polynomials used in flattening of AFM images [27].

Polynomial	Description
$z = a$	The zero polynomial, which centers data on every scan line of the images
$z = a + bx$	Order one polynomial; it computes the offset (a) and slope (b) and deducts it from the center data of each scan line
$z = a + bx + cx^2$	Order two polynomial, which centers the data, computes the least square fit of the polynomial and then substrates it from the scan line to remove the tilt and bow on the scan lines.
$z = a + bx + cx^2 + dx^3$	The least square fit of the third order is calculated and then subtracted from the scan line to remove tilt and bow.

fit polynomials on each scan line to correct the unwanted features of the image. It uses a mathematical equation (polynomial) to model the average image surface and then subtracts the average from the surface of the image. The centre data, taken as the 0th order, is used as the datum while anything in the orders of 1st, 2nd, 3rd, and so forth is taken as the tilt. The best fit polynomial for each scan line of the required order is determined and then deducted from the centre data for every trace and retrace. There are four important polynomials used during flattening processing of images in Bruker Nanoscope software. These polynomials are explained in Table 9.2. Plane fitting, on the other hand, removes the artefacts associated with thermal drift, lateral noise and vibrations of the cantilever during AFM imaging. It calculates a single polynomial for an image and subtracts it uniformly from the image in the X- or Y-directions. The pre-processing stage should be undertaken carefully to avoid introduction of image processing artefacts such as levelling and filtering artefacts onto the AFM image [27].

9.3.3.2 Section Analyses

The processed images were then exported to Gwyddion version 2.50 for image analysis. The software is purposely designed to analyze the height fields of structures captured by STM, AFM and other SPM methods. A large number of data processing functions of this software makes it possible to

undertake a series of analyses, including statistics, data correction, profile extractions and filtering. In our case, the AFM images were first cropped to remove the unwanted sections including the scale bar and imaging parameters and then converted to grayscale. The scaling of the image, based on the AFM settings (on the scale bar), was performed for accurate measurements of the height and horizontal values. Then, a line profile analysis was undertaken using the profile extract function across the section on all the images to quantify the periodic nature and morphological properties of the thin aluminum films.

9.3.3.3 Fast Fourier Transformation (FFT)

To compute the power spectrum, the images were analyzed using a step by step *m-script* code written in MATLAB® R2017b. The script uses the '*imread*' function to upload the image into the MATLAB environment. The '*imshow*' function is used to plot the original image (since it does not include the axes). The function is used when no further processing has been undertaken on the image. The '*rgb2gray*' function was used to convert the coloured 2D AFM images into grayscale. To transform the images into the frequency domain, 2D fast Fourier transform (FFT) algorithm was used. The FFT is described by Zhu *et al.,* [25] as follows. If the grayscale function of the original 2D image is $f\left(r\right)$ and r defines the positional coordinate in 2D dimensional space, then the power spectrum $p\left(k\right)$ of the image in the imaginary space is obtained according to Equation 9.1 as $p\left(k\right) = \left|F\left(k\right)\right|^2$ where $F\left(k\right)$ is the Fourier transform of $f\left(r\right)$ and k is the wave vectors of the image in the frequency domains. Fourier transform of an image consists of waveforms of different frequencies which when summed produce the original image.

Prior to FFT operation, the images were converted to double arrays to separate the FFT of magnitude and phase since the FFT for real and non-uniform image data is very complex. The two-dimensional Fourier transform of our images was performed using the *fft2* function. When the *fft2* operation was performed on the images, a very dark image was observed, this is because the absolute values of the 2D FFT were very large, so they could not be displayed on the 8-bit scale. There are two ways to ensure the details of the FFT image can be viewed; a function *fftshift*, which moves the lowest frequency regions of the image to the center is used followed by either a *log* function or proper scaling of the XY axes for 2D FFT images. In our case, the pixel values were scaled into logarithmic transform using the *log* function in MATLAB code to expand the range of dark pixels into the

bright region for better visibility of the Fourier transform images. For each of the images, magnitude and phase images of the Fourier transforms were generated. The magnitude FFT was generated by *imshow(abs(fftshift(fft2 (original AFM image*)))) script whereas the phase image was produced by function *'angle'* in the *fftshift* script. The magnitude image shows the most important details of the original image; the region of lowest frequencies shifted to the center of the image and highest frequency regions located away from the centre. This central region contains most of the energy and indicates many gradual changes in the original image. The phase images in Fourier domain are difficult to interpret visually because they contain very high noise. However, the phase image contains most of the important information required to construct an image; generally, most of the visual information from the original image is represented by the phase image in Fourier domain. The magnitude image consists of wavelengths of contrasts of pixels in the original image. As such, magnitude images are used to quantitatively explain the gradual changes in the original images. The 2D magnitude images consist of four quadrants power spectra which are mirror images in both X and Y directions. The bright part of the image indicate the peaks in the power spectra and represents the intensity of the wave vectors in real space of the image. These peaks can represent the periodicities of surface structures in the actual image or can be due to the distributed noise of the scanner, especially in AFM images. The noise usually leads to unwanted peaks in FFT image and as such Fourier filtering technique can be used to modify the image in real space [7]. As such, optimization during AFM imaging and proper pre-processing of the AFM micrographs is very important to reduce artifact-related peaks.

9.3.3.4 Power Spectral Density Analysis

Finally, the power spectrum density of the images was computed from the FFT magnitude data using Equation 9.6 written as a MATLAB code and then a plot of PSD vs frequency was generated from this data. PSD data from real images is usually very noisy and non-even and therefore smoothening is necessary. In this work, ORIGIN 2018b software was used to smoothen (and filter noise) the PSD vs frequency data. As illustrated in the literature [7], PSD profiles are usually symmetrical and data on the left is a mirror of the one on the right-hand side. For simplicity, only the right-hand data for the PSD profiles were presented in this work. The smoothened data was then exported to MATLAB code for repploting of PSD profiles. The experimental data on PSD was then fitted into the two PSD models; k-correlation (ABC) and inverse power law model described in Equations 9.7 and 9.8.

ABC correlation represents a nonlinear mathematical model consisting of three constants A, B and C as earlier described in this article and therefore fitting data on this kind of model would require nonlinear regression executed in a MATLAB script. To achieve this, a function script of the ABC correlation was written as a linear model (using logarithmic conversions) in *m-file* and then executed using *lsqcurvefit* function to fit the experimental PSD data. The process is iterative and involved the repetitive choice of initial values of the constants (A, B and C) until a close fit was achieved. Figure 9.6 illustrates the algorithm for power spectrum computation, construction of power profiles, curve fitting and analysis in MATLAB.

9.4 Results and Discussion

In this section, results on AFM imaging and the output of the step-by-step framework are presented with topographical information interpreted in relation to the power spectral observations and inferences made regarding the sputtering process and properties of aluminum thin films. The emphasis of this section is on the type of information and interpretations the power spectral density analysis can provide for thin aluminum films.

9.4.1 AFM Images and Line Profile Analysis

Figure 9.7 shows 2D AFM micrographs of surfaces of aluminum films deposited on Ti6Al4V substrates at rf powers of 150 W and 200 W. Their corresponding 3D micrographs obtained using Gwyddion software are also shown. The surface morphology at 200 W appears rougher with higher periodic characteristics of the structures. The periodicity of the structures at 150 W is highly clustered with some regions of the micrograph showing channels (in the 3D image) which indicate exposed parts of the substrate. This observation indicates lower sputtering yield and hence lower sputtering efficiency at low rf power 150 W.

Figure 9.8 shows the line profiles of the AFM micrographs for the films sputtered at an rf power of 150 W and 200 W on Ti6Al4V substrates. Line profiles are used to qualitatively and quantitatively describe the morphology of the surface structures. It measures both lateral and height functions of the structures as well as revealing their periodic characteristics. The periodicity of structures in thin films prepared at an rf power of 150 W is seen clustered whereas the structures formed at 200 W appear sinusoidally distributed. As noted earlier, most surfaces of metals, including aluminum, are self-affine, that means the structure contains repetitive shapes

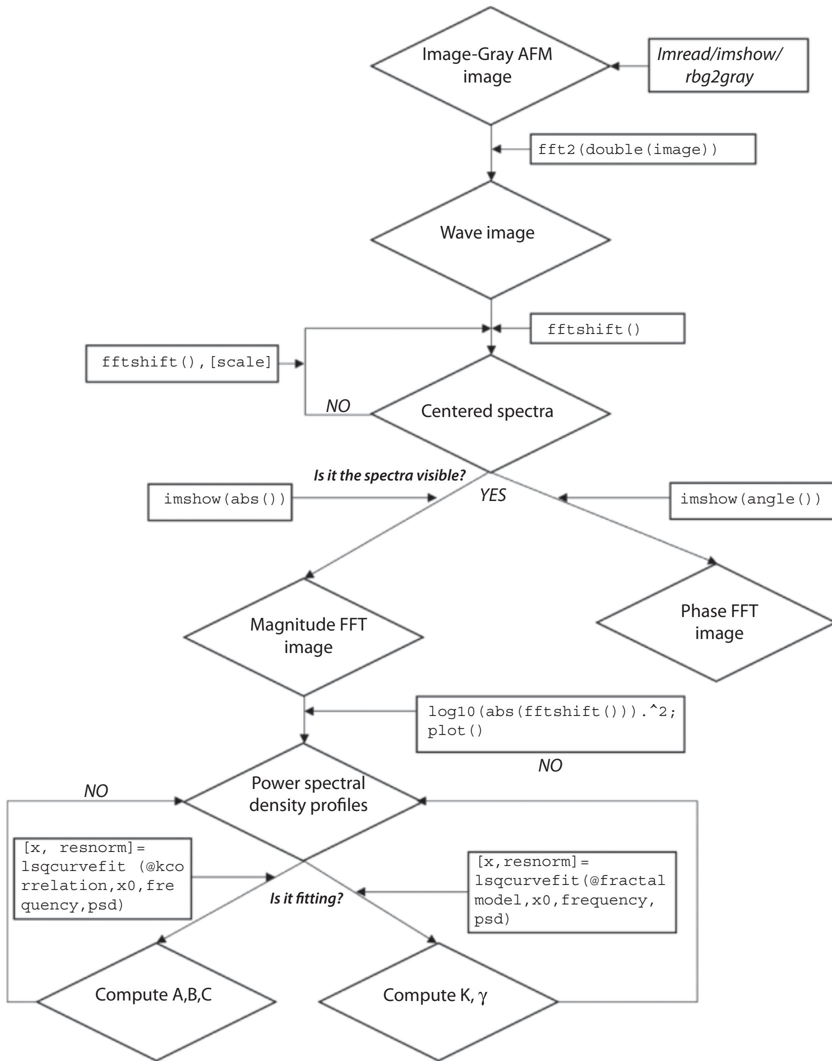

Figure 9.6 Flow chart illustrating the power spectrum algorithm implemented in MATLAB code.

under different transformation scales. The self-affine property of surface structures is the reason for periodic nature of the line profiles in this case [28]. Surfaces with such properties can, therefore, be analyzed with fractal methods such as power spectral density to determine the fractal dimensions. The PSD of self-affine surfaces follows inverse power law described

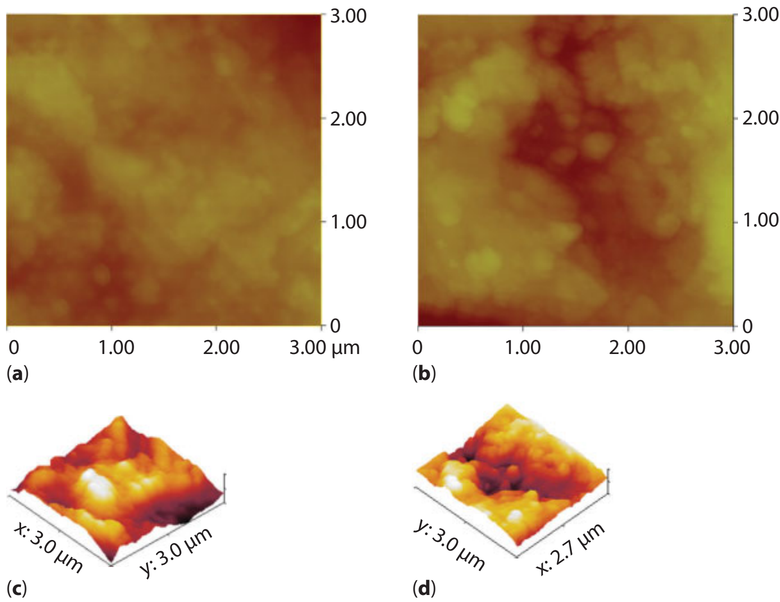

Figure 9.7 AFM micrographs of thin aluminum films deposited on Ti6Al4V at (a) 150 W and (b) 200 W and their corresponding 3D (c) (d) micrographs.

in Equation 9.8 and from this law, the fractal dimension (D) of the surface is determined as $D = 2$ for $0 \leq |\gamma| < 1$; $D = 1, 3 < |\gamma|$, otherwise, $D = \frac{1}{2}(8 - \gamma) = \frac{1}{2}[8 - (E + 2H)]$, $E = 2$. Where γ is the slope of the logarithmic plots, E is the Euclidean dimension of the Fourier transform and H is the Hurst exponent also known as the exponent of roughness [9]. The fractal dimension is used in explaining morphological and root mean square roughness transformations brought about by the changes in deposition conditions such as temperature, power and pressure [15]. The observations from these line profiles justify the application of PSD technique in analyzing the AFM images in the present work.

Figure 9.9 and Figure 9.10 show the 2D and 3D AFM micrographs and their corresponding line profiles respectively for thin aluminum films sputtered at rf powers of 150 W and 200 W on commercially pure titanium substrates. As observed in Figures 9.7 and 9.8, the surfaces are random and periodic, therefore fractal methods such as PSD can be used for their examination. The AFM images in both cases (Figures 9.7 and 9.9) clearly show the epitaxial growth mechanism of the sputtering process; nanoscale multilayer atomic additions leading to the formation of thin films [23, 29]. Line profiles are also used to show the lateral sizes of the surface structures

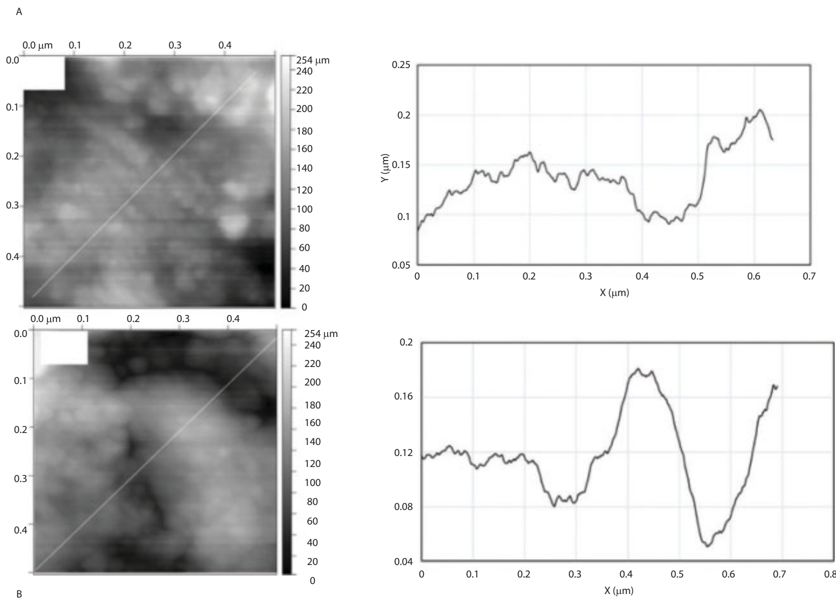

Figure 9.8 Line profiling of the surface structures of thin aluminum films deposited on Ti6Al4V at (a) 150 W and (b) 200 W.

and in this case, the profiles show larger lateral sizes of thin films prepared at 200 W. For films deposited at 200 W, the densification of the surface structures can be observed from the nature of the line profiles; the peaks are characterized by smooth tips and closer to each other as opposed to serrated tips observed at 150 W. Through visual inspection, the line profiles and three-dimensional AFM micrographs reveal the peak-to-peak arrangement as well as the layering mechanism of the surface structures.

The roughness values of the coatings were computed as presented in Table 9.3. A higher height roughness values were observed in films prepared at 200 W for all the samples. These observations can be explained by the visual examination of AFM images and line profiles in relation to the height deviation of the surface structures. The observations imply that at higher rf power (200 W in this case) larger surface structures are formed than at sputtering at lower rf power. However, as noted earlier, the spatial distribution of the surface structures may indicate otherwise.

9.4.2 Power Spectral Density Profiles

The power spectrum of the AFM images was computed to analyze the lateral distribution of the surface roughness based on the step-by-step

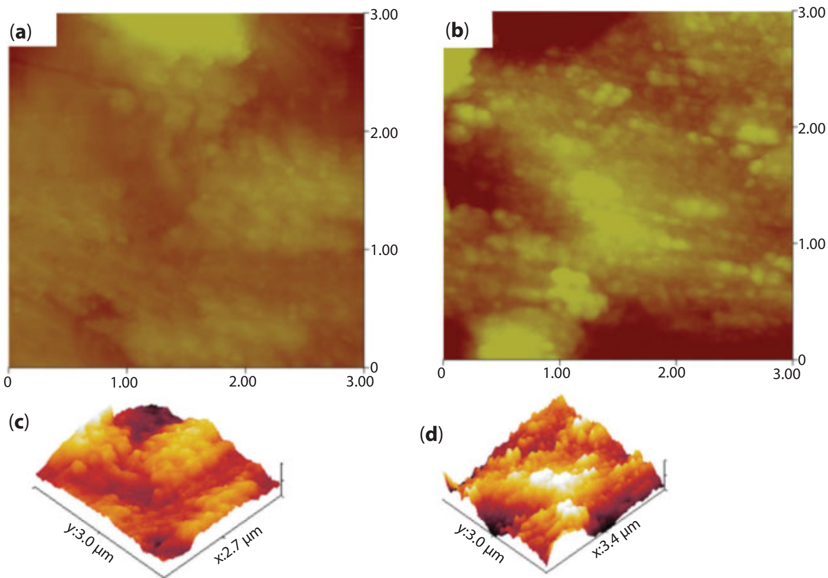

Figure 9.9 AFM micrographs of thin aluminum films deposited on commercially pure Ti at (a) 150 W and (b) 200 W and their corresponding 3D (c) (d) micrographs.

procedure illustrated in Figure 9.6. Figure 9.11 and Figure 9.12 show the output of the 2D FFT process (magnitude and phase) for thin aluminum films deposited at rf power of 150 W and 200 W on Ti6Al4V and commercially pure titanium substrates respectively.

The phase image contains information about the position of different features of the microstructure whereas magnitude image shows the energy of the frequencies of the original image. Each value on the phase image corresponds to the position of specific features on the original image and therefore it does not provide any new information about the microstructure. Therefore, the discussion in this work focused on magnitude image although it should be noted that during the reconstruction of Fourier transforms (inverse fast Fourier transform IFF), both phase and magnitude images should be used, otherwise, a blurred or corrupted image would be obtained. Considerable differences can be observed in Figure 9.11(b) , (d); the white patch at the center of the FFT image is more circular in Figure 9.11(b) than (d), which indicate sharp contrasts in the lateral arrangement of the surface structures. The periodic surfaces in the real image produce peaks in the FFT image and the values of frequency at the center of the FFT are related to the wavelengths of those periodic features. The central white vertical line in Figure 9.11(b) appears

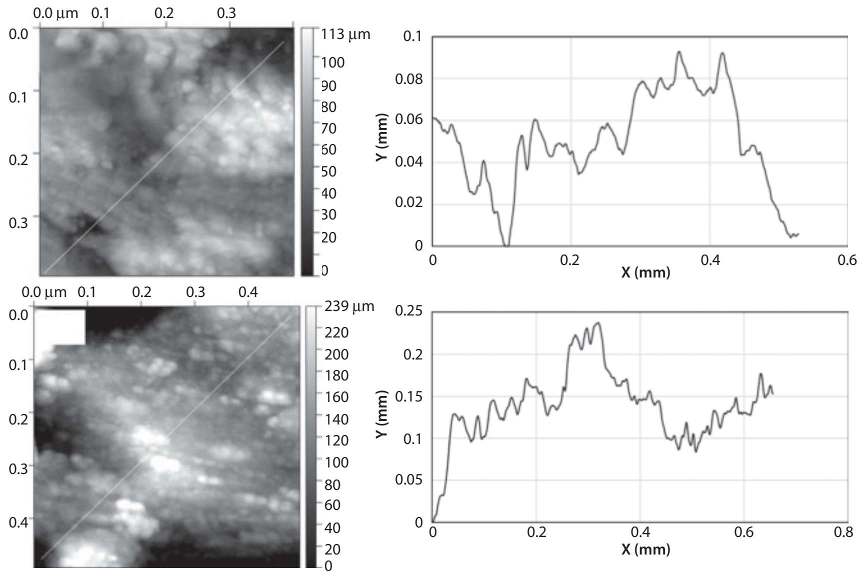

Figure 9.10 Line profiling of the surface structures of thin aluminum films deposited on commercially pure Ti at (a) 150 W and (b) 200 W.

Table 9.3 Average and root mean square roughness values for the Thin Aluminum Films from AFM images.

Samples	Al/Ti6Al4V		Al/Pure Ti	
	150 W	**200 W**	**150 W**	**200 W**
Average roughness	13.09	22.16	17.19	21.19
Root mean square	16.95	28.92	22.06	21.24

brighter, indicating dominance of horizontally-oriented surface structures at deposition power of 150 W. It further indicates uniform lateral distribution of surface structures in thin films prepared at 150 W. The FFT image in Figure 9.11(d) has sharp central horizontal and vertical white lines and dark regions away from the central region, indicating sharp contrast in lateral distribution of the surface structures of films deposited at 150 W. The high peaks visible in the high frequency (dark) regions in Figure 9.11(b) indicates the presence of spaces along the lateral structures

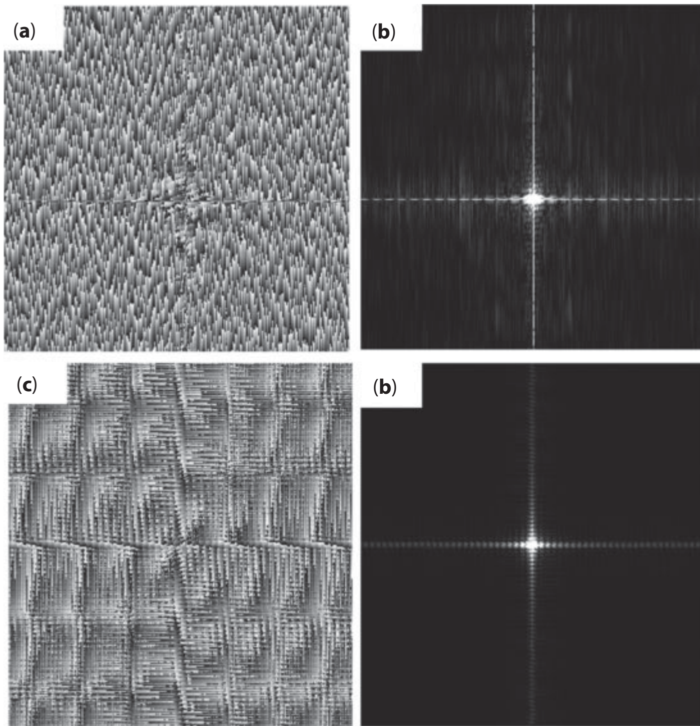

Figure 9.11 2D Fast Fourier transform (FFT) of thin aluminum films deposited on Ti6Al4V at 150 W showing (a) phase image and (b) magnitude image and at 200 W (c) phase image and (d) magnitude image.

of the film as visually observed in the 3D AFM image in Figure 9.7(c). In Figure 9.11(d), there is a clearer separation of high and low frequencies, indicating that the topography contains both very large and very fine structures. This observation is expected and agrees with the assertion that there is growth (formation) of more structures when sputtering at higher rf power. In Figure 9.12(b), the white central patch appears smaller than in Figure 9.12(d), which can be due to larger surface structures obtained at 200 W. In both cases, the dark background is clearly separated from the radial white region indicating higher lateral roughness than aluminum films deposited on Ti6Al4V and generally the surface microstructure contains of fine structures.

A detailed information of the FFT power spectra is obtained by plotting the PSD profiles in log-log axes as shown in Figure 9.13. The PSD versus spatial frequency log-log plots for all the samples exhibit typical properties with a few differences consisting of a plateau and inverse slope at low and

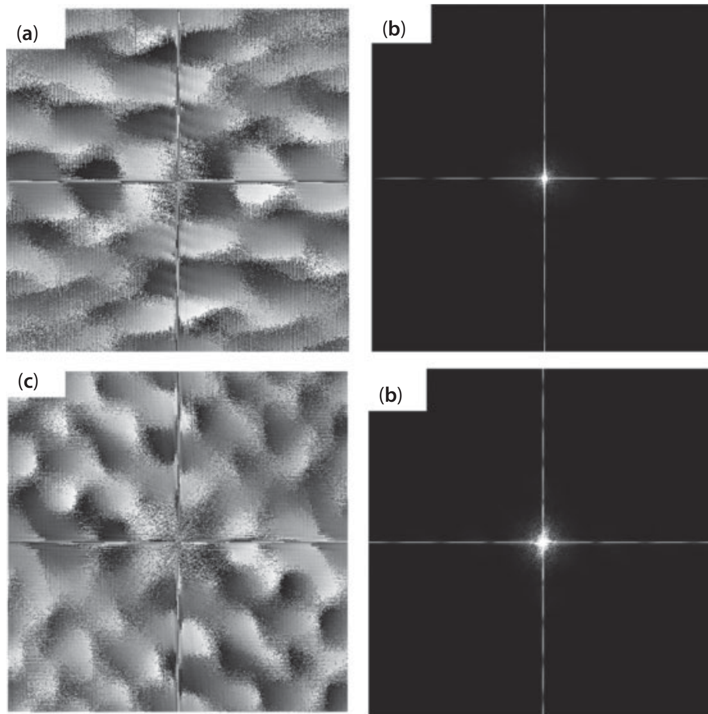

Figure 9.12 2D Fast Fourier transform (FFT) of thin aluminum films deposited on commercially pure Ti at 150 W showing (a) phase image and (b) magnitude image and at 200 W (c) phase image and (d) magnitude image.

high spatial frequencies respectively. The profiles generally show that the surface of the films deposited on different substrates exhibits 'mix' of random and periodic characteristics. This observation is reported on all the line profile analyses which show both periodic and random distribution of features in horizontal and vertical directions of the substrate surface. The transition region between low and high-frequency PSD is known as the knee and it describes the change from constant to highly correlated PSD values [9]. The plateau region illustrates the constant power spectrum density with frequency and is commonly referred to as 'white noise' region in signal processing technology. The region describes the lateral distribution of the surface structures; a large region indicates the homogeneous lateral distribution of the surface roughness. For all the samples, the flat region is observed up to spatial frequencies of about 10 nm^{-1} which is quite small indicating that all the samples are generally rough- which is expected for magnetron sputtering of aluminum films on metallic substrates [19]. The

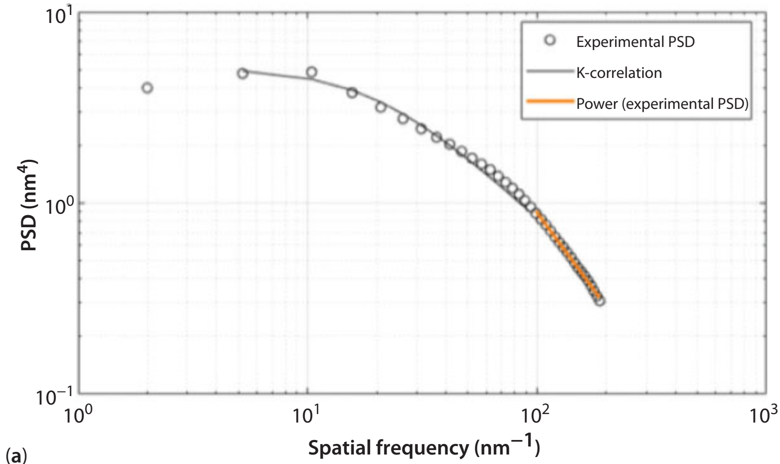

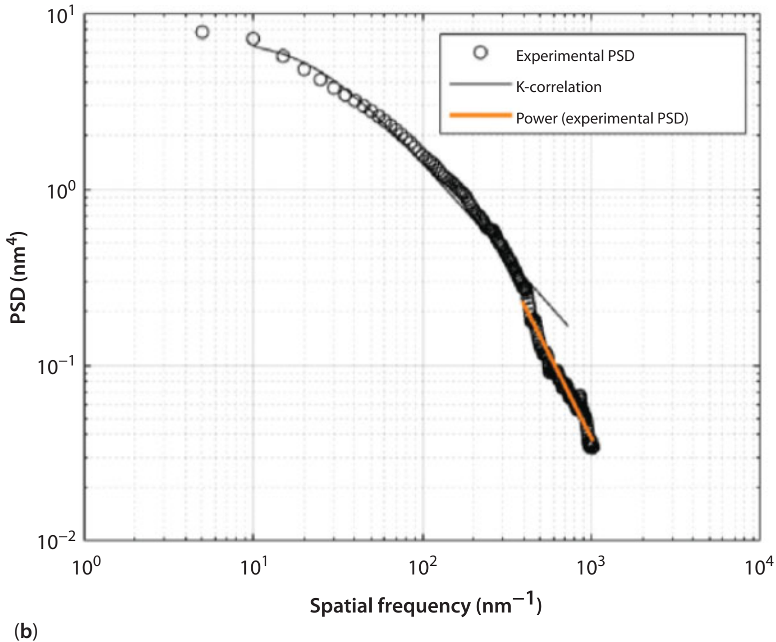

Figure 9.13 Power spectral density profiles of thin aluminum films on Ti6Al4V at (a) 150 W and (b) 200 W and on commercially pure Ti at (c) 150 W and (d) 200 W. The experimental data has been fitted on k-correlation model and inverse power law at high and low spatial frequencies respectively. (Continued)

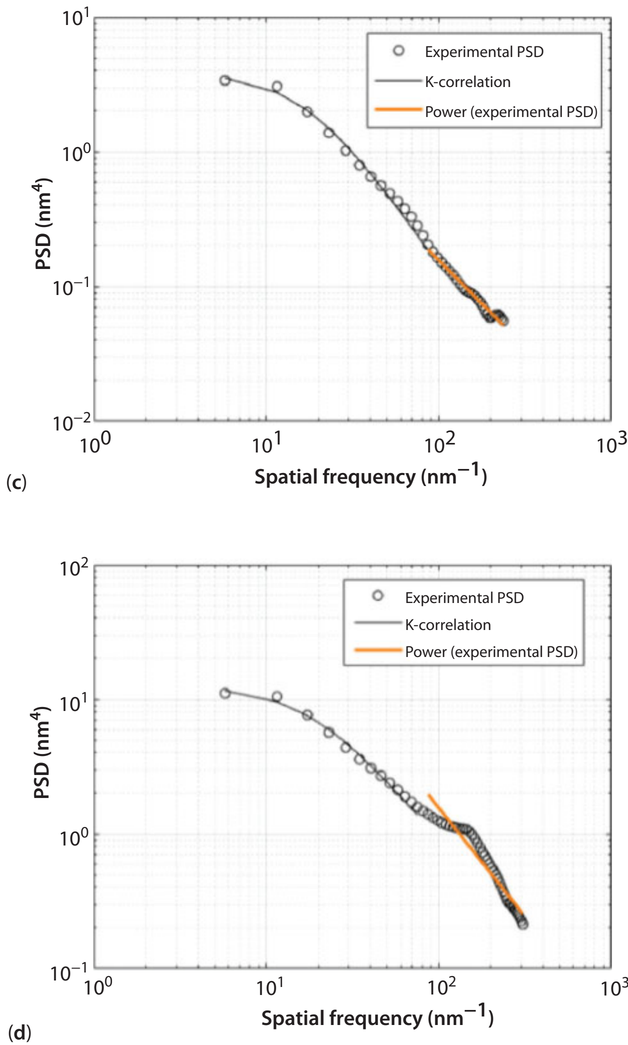

Figure 9.13 (continue)

sloping region, on the other hand, represents the highly correlated region of the PSD profiles, which is mostly described the fractal (or inverse power law) models. The existence of the two regions in the PSD profiles indicates two coexisting morphology length scales in the aluminum thin films namely microscale and nanoscale surface structures. This inference can be confirmed by the line profile measurements for all the samples that showed both scales of surface structures-it is a confirmation of the observation of

'mix' of structures in the surface morphology. The PSD profiles were fitted in k-correlation and inverse power law (fractal) models at low and high frequencies respectively as seen in Figure 9.13. The curve fitting parameters are presented in Table 9.4. The PSD profiles are dominated largely by the k-correlation model; which suggests less sharp steps on the surface structures as observed from the line profiles for all the AFM micrographs.

From Table 9.4, A is related to power density at low frequencies and increase in A indicates the larger radius of the 'white patch' in the Fourier transform the image and can be used to interpret the evolution of surface structures. The higher values of A at 200 W for both samples indicate larger structures (laterally) on the surface as it was noted from the morphological (line profile) analysis. From Table 9.4**,** B is the correlation length of the k-correlation model, which indicates the transition from peaks to valleys and vice versa. A higher value of correlation length (B) indicates lower lateral roughness, which means in this case, there was lower lateral roughness on films deposited at 200 W. The power law exponent (γ in the fractal model usually indicates the evolution of surface structures. In this case for instance, the value of power law exponent (γ) was higher at 200 W than 150 W, which may suggest growth of surface features at different wavelengths. This means the formation of more new structures as the rf power increases. The values of C in the k-correlation model describe the spectrum at high frequency; it shows the very finer and tiny details of the original image. For instance, According to Karan and Mallik [15], C determines the sizes of the surface structures and can be used to explain the growth of surface structures at different processing conditions in physical vapor deposition of thin films. From their study, we can deduce that low value of C indicates that most of the surface structures are 'large'; in this case, low C is noted at 200 W since more surface structures have evolved due to increase in rf power. From the k-correlation model curve fitting parameters, the equivalent roughness σ_{ABC} and correlation length τ were determined as earlier indicated in this chapter and have been listed in Table 9.4. These parameters are used to indicate growth of various structures during processing of thin films and their increase is an indication of evolution of surface structures for films deposited at 200 W [15]. From the inverse power law, fractal dimension (D) and Hurst component (H) values were determined and recorded in Table 9.4. Hurst values are used to determine the lateral distribution of the surface structures. According to the Hurst distribution criterion, the H values in our case are less than 0.5, indicating uniform spatial distribution of the roughness. In contrast to the apparent root mean square values in Table 9.3, the lateral roughness

Table 9.4 Fitting coefficients of the K-Correlation model and inverse power law of the PSD plots.

		k-correlation model					**Fractal/power law**			
Samples	**Power**	**A (10^3 nm)**	**B (nm)**	**C**	σ_{ABC} **(nm)**	τ	**K**	γ	**D**	**H**
	150	1.997	19.83	4.13	3.192	6.872294	1660.9	1.64	3.18	0.18
Al/Ti6Al4V	200	3.757	22.97	4.22	3.726	8.101592	2002.2	1.91	3.05	0.05
	150	1.1167	16.93	3.37	3.212	4.918131	2889.2	1.29	3.36	0.36
Al/Ti	200	3.991	17.91	3.52	5.570	5.412956	2402.9	2.02	2.99	0.01

for samples prepared at 200 W is more homogenous as compared to those prepared at 150 W.

9.5 Conclusion

A step-by-step power spectral density spectrum to analyze the surface topography of thin aluminum films prepared by magnetron sputtering has been presented in this article. The background theory and literature review of the applications of PSD in thin films was highlighted followed by a procedural description of a typical framework for PSD analysis of films. The power spectra were computed using fast Fourier transform algorithm in MATLAB script. Using thin aluminum films as the case study, the output of the framework was interpreted in relation to the sputtering process and properties of the thin films and the following conclusions can be drawn from this work.

- The method is more descriptive of the surface topography of thin aluminum films. The aluminum films deposited at 200 W were shown to have a higher average and root mean square roughness values than those deposited at 150 W according to line profile analyses. However, through the PSD analyses, films deposited at 200 W have a homogenous lateral distribution of surface structures. The finding can be explained by the fact that sputtering at higher rf power leads to the formation of larger (in terms of height) structures and generally closely packed surface features.
- Power spectral density analysis presented in this case can be used to characterize the topography of surfaces as both periodic and random. Line profiling of the AFM images in our study revealed that most of the surfaces exhibited both random and periodic surface features, which is expected for a random process such as magnetron sputtering. The surface profiling for films deposited on Ti6Al4V at 150 W revealed clustered periodicity with randomly distributed features. The PSD profiles of those specimens revealed fully random surfaces. However, the 2D-FFT analyses of these surfaces showed peaks at the high-frequency regions of the spectrum which can be interpreted as the indication of clusters of small surface features.

- The 2D-FFT image provides very important interpretations for the surface topography. The periodic features on the surface of thin films are represented as peaks in the Fourier transform image. The size of the bright central feature in FFT image represents the contrast in the lateral arrangement of the surface structures. The vertical and horizontal white lines on FFT image indicate the dominating orientation of the surface microstructure. For instance, the presence of larger radial patch on aluminum films prepared at 200 W than those prepared at 150 W is related to the formation of more and larger surface features at higher rf power.
- The PSD profiles presented in this case were all dominated by the power law with a very small white noise region (below spatial frequencies of 10^1 nm^{-1}). This finding indicates that the surfaces are highly characterized by high roughness. When k-correlation model dominates the PSD profiles, it means that the surfaces are generally smooth, whereas when the power law dominates the PSD profiles the surfaces are said to be rough.
- The curve fitting parameters from the k-correlation model are A, B and C while parameters for power law are K and γ. Each of these parameters is associated with the morphological evolution and physical process in microstructural transformation. For instance, increase in power law exponent from 150 W to 200 W films suggests growth in microstructural features at varying wavelengths. For all the cases, the power law exponent and correlation length increased from 150 W to 200 W, indicating the formation of more surface features and decrease in lateral roughness of the films at 200 W.
- The equivalent spectral length obtained from the k-correlation model can be used to approximate the surface diffusion length and activation energy during the physical preparation of metallic thin films. When there is a sudden increase in equivalent root mean square roughness and spectral length from k-correlation, it indicates that there is growth in surface structures driven by the conditions of the physical film preparation process. In our case, such increase was not observed which means that there was less, or no surface diffusion caused by rf power change from 150 W to 200 W for the two cases. The value of C in the ABC model

can be used to describe the sizes of the surface structures as it represents the PSD at very low frequencies. When C decreases, it means that there is either diffusion or aggregation of the structures resulting in larger morphological features on the surface microstructure. For all the cases, C increased from 150 W to 200 W, which means that at 200 W there is more densification of atoms onto the substrate during the sputtering process resulting in formation larger surface structures.

Acknowledgements

The authors wish to acknowledge the University Research Committee (URC), University of Johannesburg, South Africa for financing this PhD research. The authors also wish to thank Mr. Maphane Phalaneng of the Department of Physics and Astronomy, Botswana International University of Science and Technology (BIUST) for assistance with the magnetron sputtering of titanium substrates. We also thank Dr. Patrick Mubiayi for reading the first manuscript and making a positive contribution for its betterment.

References

1. Tien, C.-L., Lin, T.-W., Yu, K.-C., Tsai, T.-Y., Shih, H.-F., Evaluation of Electrical, evaluation of mechanical properties, and surface roughness of dc sputtering nickel-iron thin films,. *IEEE Trans. Magn.*, 50(7), 1–4, 2014.
2. Jiang, W.-G., Su, J.-J., Feng, X.-Q., Effect of surface roughness on nanoindentation test of thin films. *Eng. Fract. Mech.*, 75(17), 4965–4972, 2008.
3. Yoshino, H., Abbas, A., Kaminski, P.M., Smith, R., Walls, J.M., Mansfield, D., Measurement of thin film interfacial surface roughness by coherence scanning interferometry. *J. Appl. Phys.*, 121(10), 105303, 2017.
4. Rabady, R., Avrutsky, I., Alternating Bias., Radio-frequency magnetron sputtering. *J. Opt. Soc. Am.*, 20(10), 2174–2178, 2003.
5. Waterworth, A., Quantitative characterisation of surface finishes on stainless steel sheet using 3D surface topography analysis. *Thesis (Doctoral)*, 2010.
6. Eifler, M., Schneider, F., Seewig, J., Kirsch, B., Aurich, J.C., Manufacturing of new roughness standards for the linearity of the vertical axis – Feasibility study and optimization. *Eng. Sci. Technol. an Int. J.*, 19(4), 1993–2001, 2016.

7. Bowen, W.R., Doneva, T.A., Artefacts in AFM studies of membranes: correcting pore images using fast fourier transform filtering. *J. Memb. Sci.*, 171(1), 141–147, 2000.
8. Popoola, A.P.I., Fayomi, O.S.I., Popoola, O.M., Comparative studies of microstructural, tribological and corrosion properties of plated Zn and Zn-alloy coatings. *Int. J. Electrochem. Sci.*, 7(6), 4860–4870, 2012.
9. Gong, Y., Misture, S.T., Gao, P., Mellott, N.P., Surface roughness measurements using power spectrum density analysis with enhanced spatial correlation length. *J. Phys. Chem. C*, 120(39), 22358–22364, 2016.
10. Xu, C., Tian, H., Reece, C.E., Kelley, M.J., Topographic power spectral density study of the effect of surface treatment processes on niobium for superconducting radio frequency accelerator cavities. *Phys. Rev. ST. Accel. Beams*, 15(4), 2012.
11. Gavrila, R., Dinescu, A., Mardare, D., A power spectral density study of thin films morphology based on AFM profiling. *Rom. J. Inf. Sci. Technol*, 10(3), 291–300, 2007.
12. Senthilkumar, M., Sahoo, N.K., Thakur, S., Tokas, R.B., Characterization of microroughness parameters in gadolinium oxide thin films: A study based on extended power spectral density analyses. *Appl. Surf. Sci.*, 252(5), 1608–1619, 2005.
13. Jacobs, T.D.B., Junge, T., Pastewka, L., Quantitative characterization of surface topography using spectral analysis. *Surf. Topogr. Metrol. Prop.*, 5(1), 013001, 2017.
14. Wojciechowski, S., Twardowski, P., Chwalczuk, T., Surface roughness analysis after machining of direct laser deposited tungsten carbide. *J. Phys. Conf. Ser.*, 483(1), 012018, 2014.
15. Karan, S., Mallik, B., Power spectral density analysis and photoconducting behavior in copper(II) phthalocyanine nanostructured thin films. *Phys. Chem. Chem. Phys.*, 10(45), 6751, 2008.
16. Persson, B.N., Albohr, O., Tartaglino, U., Volokitin, A.I., Tosatti, E., On the nature of surface roughness with application to contact mechanics, sealing, rubber friction and adhesion. *J. Phys. Condens. Matter*, 17(1), R1–R62, 2005.
17. Anandhan, S., Mapping of thermoplastic elastomeric nitrile rubber / poly (styrene-co-acrylonitrile) blends using tapping mode atomic force microscopy. *J. Mater. Sci.*, 8(13), 2793–2801, 2003.
18. Buchko, C.J., Kozloff, K.M., Martin, D.C., Surface characterization of porous, biocompatible protein polymer thin films. *Biomater. Biomater*, 22(11), 1289–1300, 2001.
19. Mwema, F.M., Oladijo, O.P., Sathiaraj, T.S., Akinlabi, E.T., Atomic force microscopy analysis of surface topography of pure thin aluminum films. *Mater. Res. Express*, 5(4), 046416–15, 2018.
20. Datta, J., Bhattacharya, C., Bandyopadhyay, S., Cathodic deposition of CdSe films from dimethyl formamide solution at optimized temperature. *Appl. Surf. Sci.*, 253(4), 2289–2295, 2006.

21. Ponomareva, A.A., Moshnikov, V.A., Suchaneck, G., Microstructural characterization of hierarchical structured surfaces by atomic force microscopy. *IOP Conf. Ser. Mater. Sci. Eng.*, 47, 012052, 2013.
22. Aurongzeb, D., Growth instability and surface phase transition of Ti thin film on Si(111): An atomic force microscopy study. *Appl. Surf. Sci.*, 252(18), 6135–6140, 2006.
23. Mwema, F.M., Oladijo, O.P., Akinlabi, S.A., Akinlabi, E.T., Properties of physically deposited thin aluminium film coatings: A review. *J. Alloys Compd.*, 747, 306–323, 2018.
24. Erinosho, M.F., Akinlabi, E.T., Estimation of surface topography and wear loss of laser metal-deposited TI6Al4V and Cu. *Adv. Eng. Mater.*, 18(8), 1396–1405, 2016.
25. Zhu, J., Balieu, R., Lu, X., Kringos, N., Microstructure evaluation of polymer-modified bitumen by image analysis using two-dimensional fast Fourier transform. *Mater. Des.*, 137(5), 164–175, 2018.
26. Mwema, F.M., Mbuya, T.O., Mose, B., Keraita, J.N., Microstructural and micro hardness characterization of primary and recycled cast al-sipiston alloys processed by high-pressure torsion. Msc. Thesis, Department of Mechanical Engineering, Jomo Kenyatta University of Agriculture & Technology, 2015.
27. Eaton, P., West, P., *Atomic Force Microscopy*. New York, NY, Oxford University Press Inc, 2010.
28. Khamesee, M.B., Kurosaki, Y., Matsui, M., Murai, K., Nanofractal analysis of material surfaces using atomic force microscopy. *Mater. Trans.*, 45(2), 469–478, 2004.
29. Odetola, P.I., Popoola, P.A.P., Oladijo, P., Thin coating deposition by magnetron sputtering. Hershey, (Ed.),. *Production, Properties, and Applications of High Temperature Coatings, A. H. Pakseresht*. Pennsylvania, IGI Global. pp. 403–428, 2018.